

# Improved Infrared Light Management with Transparent Conductive Oxide/Amorphous Silicon Back Reflector in High-Efficiency Silicon Heterojunction Solar Cells

Weiyuan Duan,\* Karsten Bittkau,\* Andreas Lambertz, Kaifu Qiu, Zhirong Yao, Paul Steuter, Depeng Qiu, Uwe Rau, and Kaining Ding

To improve the infrared (IR) response, a high-refractive-index intrinsic amorphous silicon (a-Si:H) layer is introduced after metallization of bifacial silicon heterojunction (SHJ) solar cells, resulting in a transparent conductive oxide (TCO)/a-Si:H back reflector, which functions like distributed Bragg reflector (DBR). This concept is demonstrated by both Sentaurus Technology Computer-Aided Design (TCAD) simulation and experimental methods. The TCO/a-Si:H back reflector can increase rear internal reflectance by reducing the transmission loss, thus improving the IR external quantum efficiency. The using of Sn-doped In<sub>2</sub>O<sub>3</sub> (ITO)/a-Si:H back reflector in >23.5% efficiency SHJ solar cells can improve short-circuit current density by 0.4 mA cm<sup>-2</sup> which is quite similar as using the more expensive ITO/Ag back reflector, while keeping a cell bifaciality of 55%. This brings its advantage for monofacial application case. Future studies would be nice to work on higher transparent back reflectors to broaden the application in bifacial case. This back-reflector design promotes IR response of SHJ solar cells with transferring to a wide variety of TCOs.

## 1. Introduction

Silicon heterojunction (SHJ) solar cells coupled with hydrogenated intrinsic amorphous silicon (a-Si:H) enable high open-

Dr. W. Duan, Dr. K. Bittkau, Dr. A. Lambertz, Dr. K. Qiu, Z. Yao, P. Steuter,

D. Qiu, Prof. U. Rau, Dr. K. Ding
IEK-5 Photovoltaik
Forschungszentrum Jülich GmbH
52425 Jülich, Germany
E-mail: w.duan@fz-juelich.de; k.bittkau@fz-juelich.de
Dr. K. Qiu, Z. Yao
Institute for Solar Energy Systems
Guangdong Provincial Key Laboratory of Photovoltaic Technology
School of Physics
Sun Yat-Sen University

The ORCID identification number(s) for the author(s) of this article can be found under https://doi.org/10.1002/solr.202000576.

© 2021 The Authors. Solar RRL published by Wiley-VCH GmbH. This is an open access article under the terms of the Creative Commons Attribution-NonCommercial-NoDerivs License, which permits use and distribution in any medium, provided the original work is properly cited, the use is noncommercial and no modifications or adaptations are made.

DOI: 10.1002/solr.202000576

510006 Guangzhou, P.R. China

circuit voltages ( $V_{oc}$ ) of up to 750 mV.<sup>[1]</sup> Recently, Hanergy demonstrated a new bifacial SHJ record with certified efficiency of 25.11% from one side illumination.[2] The impressive 84.98% fill factor (FF) has eliminated the fears that SHI solar cell could not reach high FFs. [3,4] However, the short-circuit current density ( $J_{sc}$ ) of 39.55 mA cm<sup>-2</sup> was much lower compared with the other two sides contacted silicon champion solar cells, like passivated emitter and rear contact cell or tunnel oxide passivated contacted solar cell, which have a  $J_{\rm sc}$  above 40 mA cm<sup>-2</sup>.<sup>[5]</sup> Consequently, increasing  $J_{\rm sc}$  is a more promising route to further improve SHJ device efficiency.

Previous studies mostly focused on reducing parasitic absorption in the front a-Si:H layers or transparent conductive oxide (TCO) layers in the SHJ solar cells to improve  $I_{\rm sc}$ . [6–12] These researches

mainly considered the optical losses of short-wavelength light. In addition, all the solar cells have poor conversion efficiency for light with wavelengths near the active-layer bandgap, where photons with energy near the bandgap can travel long distances (many times the substrate thickness) without being absorbed. [13] Thus, light-trapping at the near-bandgap wavelengths, which minimizes the portion of escaped light to increase infrared (IR) response, could also contribute to I<sub>sc</sub> improvement of SHJ solar cells.<sup>[14]</sup> Furthermore, the IR light management becomes increasingly important as the wafer thickness is reduced which is expected as the only way for further significant improvement in  $V_{oc}^{1,[15,16]}$  The transmittance loss at long wavelengths for bifacial SHJ solar cells is mainly caused by photons with energy near the bandgap that intersect the rear side of the solar cell within the escape cone, thus not being reflected by TCO and getting lost. [17] To confine the escaped light, a better back reflector is needed to reflect the light back from the rear side so that more light can be trapped in the silicon absorber.

For the IR light management in SHJ solar cells, full area Ag together with TCOs typically act as a back reflector has often been used. [18,19] However, except the expensive price of Ag, such a structure can easily bring plasmonic absorption at the TCO/metal interface induced by the parallel-polarized light of evanescent waves impinging on the metal surface which excites

www.advancedsciencenews.com



www.solar-rrl.com

surface plasmons. [20,21] In this work, instead of Ag, a cheaper intrinsic a-Si:H layer was introduced after metallization of bifacial SHI solar cell, resulting in a TCO/a-Si:H back reflector. Unlike sophisticated light management structures in solar cells such as diffraction gratings, black silicon or other kind of nanophotonics, TCO/a-Si:H back reflector has a function like distributed Bragg reflector (DBR), the DBR structure is easy to be fabricated and has been demonstrated in the application of crystalline silicon solar cells. [22–28] Sputtered indium tin oxide (ITO) was chosen in this work because it is the most common used TCO in heterojunction solar cells, making it a model system. Sentaurus Technology Computer-Aided Design (TCAD) simulation was carried out for the optics in terms of optimizing the thickness of ITO/a-Si:H stack. We systematically investigated how the ITO/a-Si:H back reflector increases rear internal reflectance by measuring external quantum efficiency (EQE) and reflectance (R) before and after deposition of the a-Si:H layer. Finally, I<sub>sc</sub> improvement was compared between using ITO/ a-Si:H and ITO/Ag back reflector, and the bifaciality of the cells were also discussed.

## 2. Results and Discussion

#### 2.1. TCAD Simulation

To quantify the optical performance of the solar cell with intrinsic a-Si:H layer integrated on the rear side in terms of  $J_{\rm sc}$ , simulations using Sentaurus TCAD were carried out for the complete layer stack, as shown in **Figure 1**, without considering the shading or plasmonic absorption from front and rear silver grids. Normally, a DBR consists of layers with alternating high and low refractive indices. In our case, light impinges from the c-Si wafer to the interface with ITO, which has a low refractive index ( $\approx$ 2.0 at 1000 nm), followed by a-Si:H with high refractive index ( $\approx$ 3.2 at 1000 nm). Finally, the air half space has a low refractive index. Typically, DBRs consist of much more alternating layers to ensure a highly reflective wavelengths band. Being

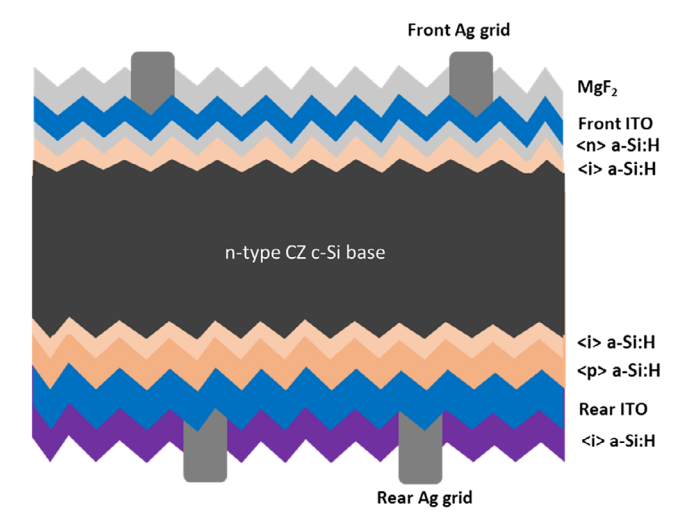


**Figure 1.** Cross-sectional sketch of the bifacial SHJ solar cell in rear emitter configuration.

part of an electro-optical device, like in our case, such a DBR needs to be reduced respect to the number of layers to avoid resistive losses, since vertical extraction of photogenerated charge carriers suffers by adding more and more layers at the back side. Here, we sandwiched ITO/a-Si:H between c-Si and air as a back reflector. These two layers are expected to not increase the resistive loss but take the advantage of the principle of DBR. To maximize the optical improvement, the thicknesses of the ITO and a-Si:H layers need to be aligned according to the wavelengths that mostly gain by advanced light management. In general, the desired layer thicknesses depend on the angle of incidence as well as the absorption probability of reflected photons. If the absorption probability is too low, the absolute gain in  $I_{sc}$  will be low, as photons will get lost by reflection instead of being lost by transmission. In contrast, if absorption probability is too high, the number of photons reaching the back reflector will be very low. Therefore, the impact of increased reflectivity on current generation will be low. Both, wafer thickness and surface texture, have an impact on the wavelength and angular range, for which light management needs to be improved. Therefore, the thicknesses of ITO and a-Si:H layers need to be designed for the real solar cell structure

By varying the rear ITO and outermost intrinsic a-Si:H layer thicknesses in our bifacial SHJ solar cells, color maps of  $J_{\rm sc}$  generated in solar cells with different wafer thicknesses are shown in **Figure 2**. Both wafers show a very similar  $J_{\rm sc}$  evolution trend according to the variation of ITO and a-Si:H thickness. As one can see, for each ITO layer thickness, a different value for the optimal intrinsic a-Si:H layer thickness is found. This demonstrates that interference takes place in both layers together. The almost elliptic shape in the color map can be understood as an effect of a DBR, where the optical path length through the layers with alternating refractive indices has to match half the wavelength of incident light to achieve constructive interference in reflection. This means that reflection properties are less sensitive to thickness changes when the combined optical path length is kept constant.

The optimum double layer back reflector coating is positioned at ITO thickness of 140 nm and a-Si:H thickness of 90 nm regardless of wafer thickness. Compared with solar cells only with standard 70 nm rear ITO, the optimized ITO/a-Si:H back reflector could bring 0.84 and 0.77 mA cm $^{-2}$  gain for wafer thickness of 130 and 170  $\mu m$ , respectively. The slightly higher gain for 130  $\mu m$  wafers also confirms that light management becomes more important for thinner wafers.

To figure out how the TCO/a-Si:H back reflector boosts the generated  $J_{\rm sc}$ , a detailed analysis of the impact from each layer was carried out with or without introducing a-Si:H. Figure 3 shows the reflection and absorption spectra of the different layers placed on the front and rear sides of a 130  $\mu$ m wafer. The figures have been divided into several regions according to the loss mechanism, and the current of each region has been calculated by integrating over AM 1.5 G photo flux density. Individual current divided by total loss gives the proportion of each part. In the reference layer stack with 70 nm ITO on the rear side, the 4.02 mA cm<sup>-2</sup> transmittance loss accounts for the largest portion, which already exceed more than 50% of the total loss, as shown in Figure 3a. The use of an optimized TCO/a-Si:H back

www.solar-rrl.com

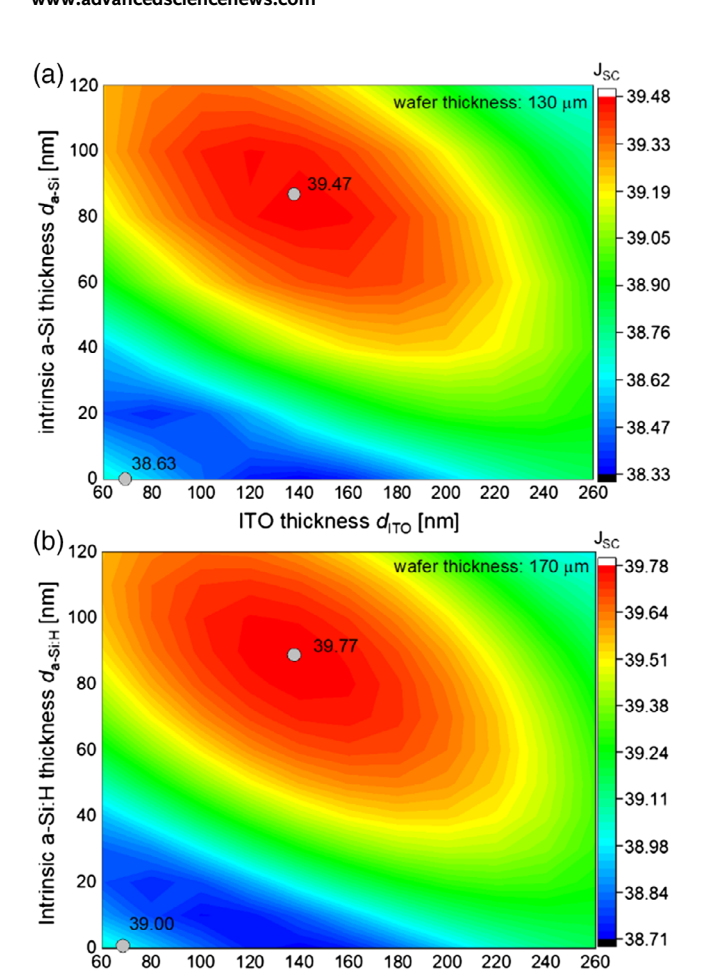


**Figure 2.** Simulated color maps of current density  $J_{sc}$  generated in the SHJ solar cells based on wafer thickness of a) 130  $\mu$ m and b) 170  $\mu$ m, without considering grids effect.

ITO thickness d<sub>ITO</sub> [nm]

reflector reduces the transmittance loss significantly by 1.57 mA cm<sup>-2</sup>, as shown in Figure 3b. The reduced transmittance is mainly transferred to generated  $J_{\rm sc}$  (+0.84 mA cm<sup>-12</sup>) and increased reflectance ( $+0.71 \text{ mA cm}^{-12}$ ). This demonstrates the performance of the additional intrinsic a-Si:H layer as part of the back reflector. Even though an increased reflection will cause a longer-distance travel of the light in the cell, the parasitic absorption of front and rear ITOs only slightly increase thanks to their high optical quality. We emphasize that the simulations depicted here could deviate from the experiments, as the shading loss and plasmonic absorption from front and rear grids are not considered. The possible contribution from photogenerated carriers in a-Si:H layers is also not included. [ $^{[29]}$  Moreover, the nand k values are extracted from thick layers on glass which most likely have properties deviating from those of the thin layers used in the cell. Nevertheless, the simulation results verified the importance of using back reflector in SHJ solar cells.

#### 2.2. Solar Cells

Based on the optical simulation, we prepared SHJ solar cells following the optimized simulated designs as discussed earlier, using 140 nm ITO and 90 nm a-Si:H as a combination on the rear side. For comparison, original SHJ solar cell with standard 70 nm rear ITO was prepared as reference, meanwhile solar cells with 70 nm ITO and 200 nm Ag were also fabricated. Figure 4 shows the relative change of cell performance after introducing ITO/a-Si:H or ITO/Ag back reflector, based on a group of five cells each. Both types of the cells show about 1% Isc improvement, where the maximum absolute increase is 0.46 and 0.4 mA cm<sup>-2</sup> for cells with ITO/Ag and ITO/a-Si:H back reflector, respectively. There is no compromise for  $V_{oc}$  when introduce back reflectors, no matter for a-Si:H or Ag. The change of FF for cells combined with full area back a-Si:H presents fluctuations with a deviation between -0.5% and 0.5% which lies within the typical dispersion of our process, material and measurement. This also demonstrates that this ITO/a-Si:H two-layer structure which has the DBR function does not increase the resistive loss. However, the using of full area back Ag causes a relatively higher fluctuation of FF with an absolute value more than 1%. We speculate this could be aroused from the stability of rear contact during the measurement. Overall, the I<sub>sc</sub> gain eventually drives the efficiency increase, leading up to 1.01% abs gain when using ITO/a-Si:H back reflector. For the cells with ITO/Ag back reflector, the efficiency improvement is affected by both  $I_{sc}$ and FF which shows a wide variation between 0% and 2%. Nevertheless, the average gain values for both types of cells are quite close, which demonstrate the concept of using ITO/a-Si:H as a back reflector in SHJ solar cells.

To further figure out the DBR function of ITO/a-Si:H stack, EQE and 1-R spectra before and after a-Si:H deposition are shown in Figure 5 with rear ITO thickness of 140 nm. Apparently, the source of the  $J_{sc}$  enhancement is the superior internal reflectance of the ITO/a-Si:H reflector, which simultaneously increases EQE and escape reflectance. The area between the EQE and 1-R curves accounts for the parasitic losses from absorption in the thin layers as well as from transmission. It can be seen that the total loss from IR parasitic absorption and transmittance is reduced in case of the ITO/a-Si:H back reflector. This shows the successful transfer from elsewise transmitted photons to generated charge carriers in the c-Si wafer, without suffering from significant parasitic absorption. Please note that, the comparison shown in Figure 5 is done on exactly the same device before and after deposition of the a-Si:H layer at the rear side. Therefore, the effect of the a-Si:H back layer could be shown without suffering from batch-to-batch fluctuations typically happening during layer deposition, as all other layers remain identical.

SHJ technology is bifacial by nature due to the transparent front and rear sides of the solar cells. This bifaciality could improve the energy yield and reduce the levelized cost of electricity. To figure out if the introduced back reflector contradicts the improved energy yield by the bifaciality, detailed analysis was carried out between original SHJ solar cells (with only ITO on the rear side) and cells with different back reflector mechanisms. The representative parameters of different cell types, here referred to original SHJ solar cells with 70 nm ITO on the rear side, cells with ITO/a-Si:H back reflector and cells with ITO/Ag back reflector illuminated from both sides are shown in **Table 1**. The original SHJ solar cell shows a bifaciality of 86%, which is in good agreement to reported values on SHJ solar cells. The

www.advancedsciencenews.com www.solar-rrl.com

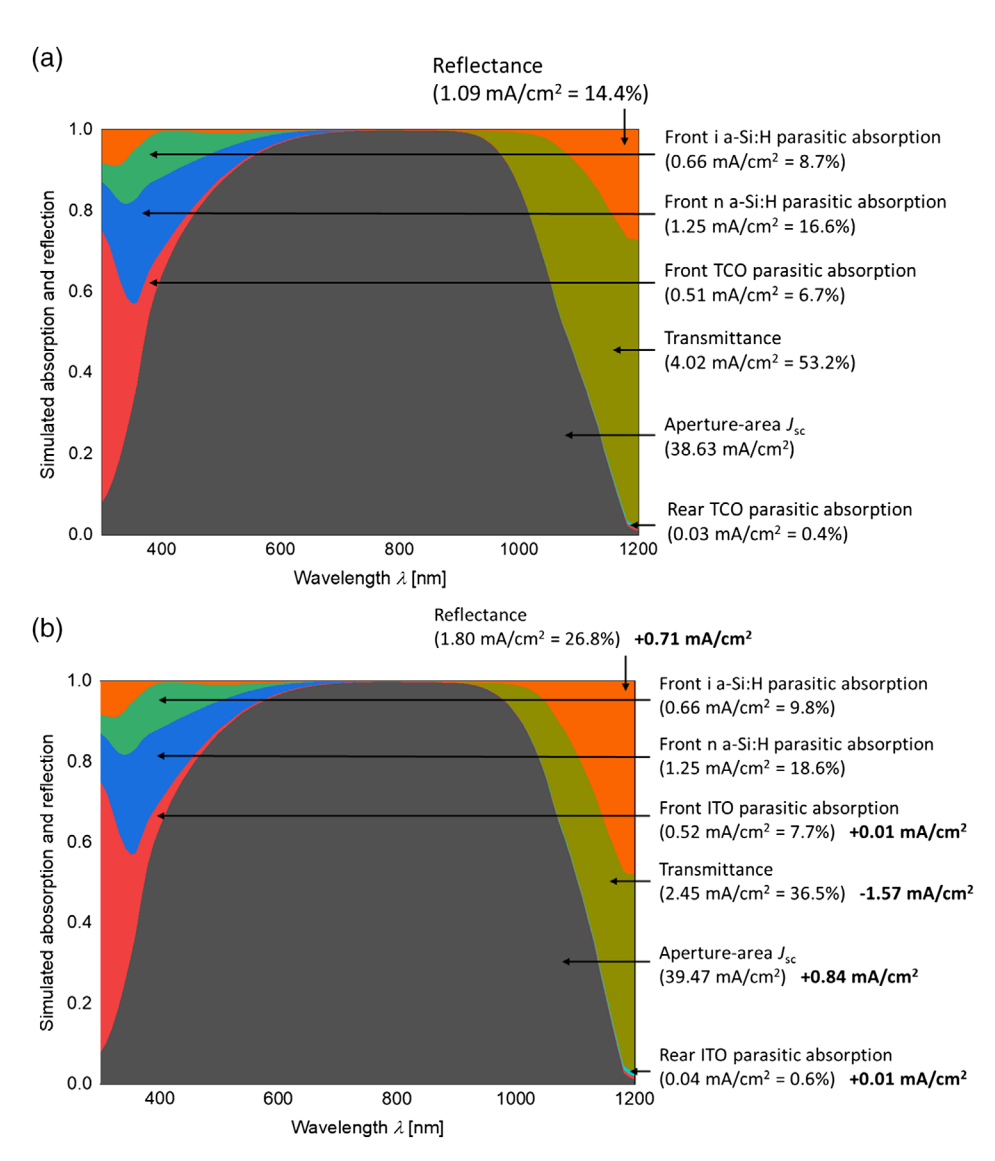


**Figure 3.** Simulated absorption and reflection spectra for SHJ solar cell stacks with a) 70 nm ITO, b) 140 nm ITO and 90 nm a-Si:H on the rear side based on 130  $\mu$ m-thick wafers. The detailed layers are shown in Figure 1 without considering front and rear grids. The aperture-area  $J_{sc}$  and equivalent current associated with each loss mechanism were calculated by integrating over the AM 1.5 G photon flux density. The number after each current loss mechanism is the ratio divided by total loss.

introduction of a-Si:H or Ag on the rear side will promote the same improvement of generated  $J_{sc}$  illuminated from the front side, thus similar gain in cell efficiency. However, ITO/Ag back reflector makes SHJ solar cell as a monofacial structure and eliminate its bifacial advantage. In contrast, the using of ITO/a-Si:H back reflector still maintains a bifaciality of 55%, as the a-Si:H is not totally opaque. For a monofacial application case, cells with ITO/a-Si:H back reflector have the advantage among these three methods as it gives higher efficiency than original SHJ solar cell and lower cost compared with cells with ITO/Ag reflector. However, the original SHJ solar cell is still the best choice for a bifacial application. Even though a solar cell with ITO/a-Si:H back reflector has a higher conversion efficiency from the front side, the dramatic drop of bifaciality from 86% to 55% only shows an advantage in a bifacial application when the rear illumination is lower than 3.6% of the front illumination intensity. This value comes from an approximate calculation which assumes the total current generation is the sum of the front illuminated current plus the rear illuminated current generation. Future work would be nice to work on higher transparent back reflectors to generate higher  $J_{\rm sc}$  without sacrificing too much bifaciality.

### 3. Conclusion

In this contribution, we have demonstrated a concept of ITO/a-Si:H back reflector implemented in SHJ solar cells by both TCAD simulation and experimental results. This ITO/a-Si:H back reflector has a function like DBR and can boost the cell performance by giving exceptional rear internal reflectance which improves the IR EQE. Unlike using ITO/Ag back reflector which

www.solar-rrl.com

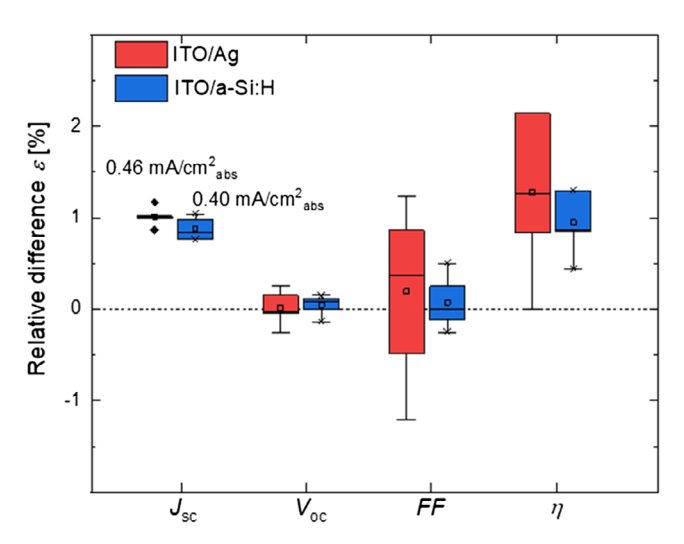


Figure 4. Relative difference of solar cell parameters after introducing ITO/a-Si:H or ITO/Ag back reflector.

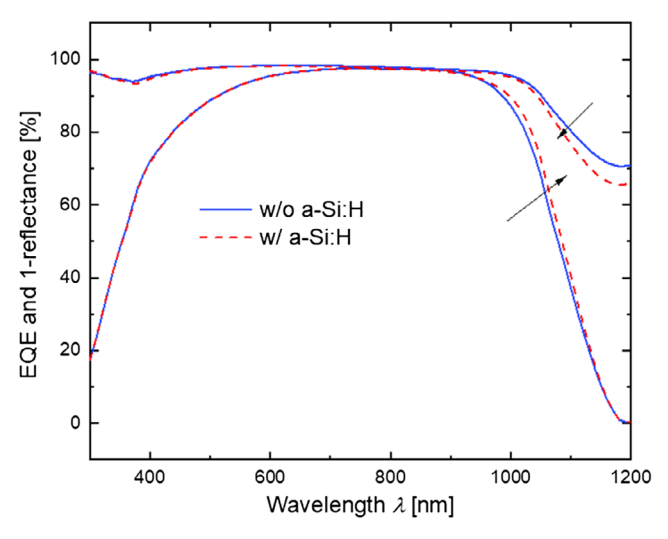


Figure 5. EQE and 1 reflectance of SHJ solar cell before (solid) and after (dashed) a-Si:H deposition.

results a bifacial SHJ solar cell into a total monofacial cell, the cheaper ITO/a-Si:H could provide a similar  $I_{sc}$  gain but maintain a bifaciality of 55%. Though cell with ITO/a-Si:H back reflector shows an advantage in the monofacial application case, the relative lower bifaciality compared with the original bifacial SHJ solar cell still limits its application in bifacial application case. Nevertheless, higher transparent back reflectors without sacrificing too much bifaciality could be further worked on in the future. Last but not the least, the reflector concept introduced here can be transferred to other cell structure with different TCOs, such as low-cost aluminum-doped zinc oxide.

# 4. Simulation and Experimental Methods

Intrinsic and doped a-Si:H layers were deposited by plasma enhanced chemical vapor deposition (PECVD) operated at



Table 1. Detailed representative device performance of original bifacial SHI solar cell, cell with ITO/a-Si:H, and cell with ITO/Ag back reflectors illuminated from front and rear sides.

Cell type	Illumination side	$J_{\rm sc}$ [mA [cm] <sup>-2</sup> ]	V <sub>oc</sub> [mV]	FF [%]	Н [%]	Bifaciality [%]
ITO	Front	39.4	738.5	80.7	23.5	86
	Rear	33.8	738.8	81.0	20.2	
ITO/a-Si	Front	39.8	739.1	80.8	23.8	55
	Rear	22.6	725.3	79.5	13.0	
ITO/Ag	Front	39.8	742.0	80.2	23.7	-
	Rear	-	-	_	-	

13.56 MHz plasma excitation frequency. ITO layers were sputtered from a vertical Von Ardenne sputter system using argon and oxygen reactive gases. For optical characterizations, a-Si:H and ITO films were deposited with a thickness of 40 and 100 nm, respectively, on glass substrates. The absorption coefficient was measured by photothermal deflection spectroscopy (PDS). The transmittance and reflectance spectra of the films were obtained using a Perkin Elmer LAMBDA 950 spectrophotometer. The thickness, refractive index (n), and extinction coefficient (k) could be obtained from ellipsometer measurement. Optical simulations were carried out using Sentaurus TCAD program with n data experimentally extracted from fitting of transmittance, reflectance, and ellipsometer results, and k data from combining the fitting result (for short wavelength) and PDS (for long wavelength). For k values of a-Si:H thin films, stitching was done at 580 nm, for ITO layer, stitching was done at 480 nm. Figure 6 shows the optical constants of each layers we have used for the simulation. The added a-Si:H(i) layer after rear ITO had the same property as front a-Si:H(i). The front and rear ITO films were also deposited under the same condition. In the simulation, a random upright pyramid texture with a spatial domain size of  $50 \times 50 \ \mu\text{m}^2$  was assumed at both, front and back, which was reconstructed from real textured wafers, measured by laser scanning confocal microscopy. For the optical simulation, raytracing model with Monte Carlo method was used. Lateral boundaries were assumed as reflecting. Transfer Matrix method was applied to consider front and back layer stacks. The vertical boundary at the front was assumed to be open, whereas absorbing boundary was chosen at the back. This way, escaped light rays described the reflectance, while light rays absorbed at the boundary described the transmittance. In total,  $\approx$ 300 000 light rays were assumed to achieve a sufficient statistic. The current densities equivalent to the respective absorption spectra were calculated by multiplying the simulated absorption with the AM 1.5 G spectrum and integrating over the spectral region of 300-1200 nm. The current densities represented losses due to parasitic absorptions for all the layers except for the c-Si base. Grid shading, plasmonic effect, Mie-scattering from the apexes of the pyramids, and carrier collection from other layers such as the intrinsic a-Si:H, or any collection losses in the c-Si absorber were not considered in the simulation. [29] Possible deviation between simulated and experimental results could also arise from the extraction of ultrathin silicon thin-film thickness and textured wafer thickness.

www.advancedsciencenews.com www.solar-rrl.com



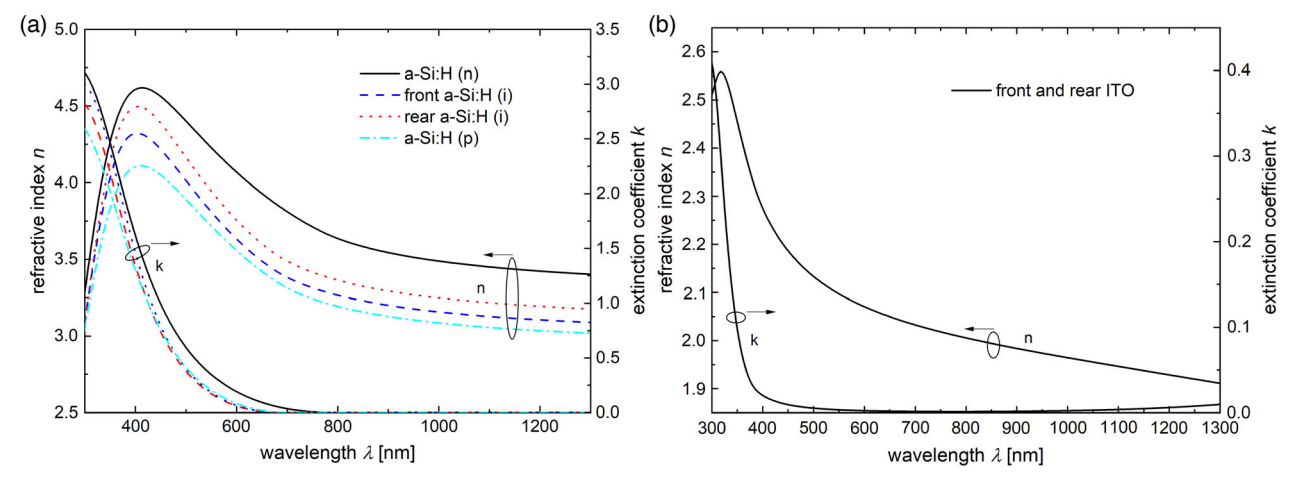


Figure 6. Optical constants of a) silicon thin films, b) ITO layers used in the TCAD simulation.

Nevertheless, these reasons for deviation will not affect the working principle of the proposed back-reflector design. The optimum combination of TCO/a-Si:H layer thicknesses will be only affected by the refractive index of each layer, which we have extracted carefully as described in the aforementioned information.

SHJ solar cells were fabricated using M2-size n-type Czochralski (CZ) silicon wafers with a thickness of 130 µm and a resistivity of 1  $\Omega$  cm. The as-cut silicon wafers were chemically etched to remove the saw damage and then textured on both sides with random pyramids in an alkaline solution. After ozone cleaning finalized with a 1% diluted hydrofluoric acid solution, intrinsic and doped a-Si:H layers were deposited via PECVD in an AK1000 cluster tool from Meyer Burger. The cell had a configuration of rear junction, where an intrinsic/ p-type a-Si:H stack was deposited on the rear side to form the hole contact (junction), and an intrinsic/n-type a-Si:H stack was deposited on the window side to form the electron contact (front surface field). ITO was sputtered from an 3% Sn-doped In<sub>2</sub>O<sub>3</sub> target onto both sides of the wafers and the layer thickness was adjusted by varying deposition time. Silver grids were screen printed on both sides of the ITO layers applying a busbarless design and subsequently cured at 170 °C for 40 min, resulting bifacial cells. Finally, very transparent MgF2 layers were sputtered on the top of the finished devices as second antireflection coating, and PECVD intrinsic a-Si:H layers were deposited on the rear side of the cells, acting, together with the ITO layer as back reflector. The whole cell structure is shown in Figure 1. For comparison, a 200 nm-thick Ag was sputtered over the entire rear surface instead of intrinsic a-Si:H, forming an ITO/Ag back reflector in the device. The current-voltage characteristics were measured under an AM 1.5 G spectrum at standard test conditions in LOANA solar cell analysis system from pv-tools with a Wavelabs Sinus 220 light source. The setup had a black chuck with low reflectivity, which has little contribution to the long wavelength reflection. Electrical contacting is achieved by mechanically pressing metal contact rails onto the fingers. Flexible wires are used as voltage sense. Furthermore, EQE and R were measured on a  $20 \times 20 \text{ mm}^2$  aperture area on the cells with fingers inside.

# **Acknowledgements**

This work was supported by the Federal Ministry of Economic Affairs and Energy in the framework of the STREET project under the grant no. 0324275E and the Helmholtz Energy Materials Foundry (HEMF) infrastructure funded by the Helmholtz Association. The authors thank Alain Doumit, Volker Lauterbach, Siekmann Hildegard, Henrike Gattermann, Silke Lynen, and Andreas Mück for technical assistance. The authors also thank their wafer supplier LONGI Co. Ltd for supporting the high-quality wafers.

Open access funding enabled and organized by Projekt DEAL.

### Conflict of Interest

The authors declare no conflict of interest.

## **Data Availability Statement**

Research data are not shared.

## **Keywords**

back reflectors, infrared responses, silicon heterojunction solar cells, transparent conductive oxide/amorphous silicon

Received: September 14, 2020 Revised: January 22, 2021 Published online:

- [1] M. Taguchi, A. Yano, S. Tohoda, K. Matuyama, Y. Nakamura, T. Nishiwaki, K. Fujita, E. Maruyama, *IEEE J. Photovolt.* **2014**, *4*, 1.
- [2] X. Ru, M. Qu, J. Wang, T. Ruan, M. Yang, F. Peng, W. Long, K. Zheng, H. Yan, X. Xu, Sol. Energy Mater. Sol. Cells 2020, 215, 110643.
- [3] A. Kanevce, W.K. Metzger, J. Appl. Phys 2009, 105, 094507.
- [4] M. Rahmouni, A. Datta, P. Chatterjee, J. Damon-Lacoste, C. Ballif, P. R. I. Cabarrocas, J. Appl. Phys. 2010, 107, 054521.
- [5] M.A. Green, E. D. Dunlop, J. H. Ebinger, M. Yoshita, N. Kopidakis, A. W. Y. Ho-Baillie, Prog. Photovolt Res Appl. 2020, 28, 3.
- [6] D. Qiu, W. Duan, A. Lambertz, K. Bittkau, P. Steuter, Y. Liu, A. Gad, M. Pomaska, U. Rau, K. Ding, Sol. Energy Mater. Sol. Cells, 2020, 209, 110471.

www.advancedsciencenews.com



- [7] A. Cruz, E. Wang, A. B. Morales-Vilches, D. Meza, S. Neubert, B. Szyszka, R. Schlatmannm, B. Stannowski, Sol. Energy Mater. Sol. Cells 2019, 195, 339.
- [8] S.Y. Herasimenka, W. J. Dauksher, M. Boccard, S. Bowden, Sol. Energy Mater. Sol. Cells 2016, 158, 98.
- [9] L. Mazzarella, S. Kirner, B. Stannowski, L. Korte, B. Rech, R. Schlatmann, Appl. Phys. Lett. 2015, 106, 023902.
- [10] Y. Zhao, L. Mazzarella, P. Procel, C. Han, G. Yang, A. Weeber, M. Zeman, O. Isabella, Prog. Photovolt. Res. Appl. 2020, 28, 425.
- [11] L. V. Mercaldo, E. Bobeico, L. Usatii, M.D. Noce, L. Lancellotti, L. Serenelli, M. Lzzi, M. Tucci, P. D. Veneri, Sol. Energy Mater. Sol. Cells 2017, 169, 113.
- [12] J. Dreon, Q. Jeangros, J. Cattin, J. Haschke, L. Antognini, C. Ballif, M. Boccard, *Nano Energy* 2020, 70, 104495.
- [13] M. A. Green, Sol. Energy Mater. Sol. Cells 2008, 92, 1305.
- [14] Z.C. Holman, M. Filipic, A. Descoeudres, S. D. Wolf, F. Smole, M. Topic, C. Ballif, J. Appl. Phys. 2013, 113, 013107.
- [15] M. A. Green, IEEE Trans. Electron Devices 1984, 31, 671.
- [16] T. Tiedje, E. Yablonovitch, G. D. Cody, B. G. Brooks, IEEE Trans. Electron Devices 1984, 31, 711.
- [17] D. Kray, M. Hermle, S. W. Glunz, Prog. Photovolt. Res. Appl. 2008, 16, 1.
- [18] Z. C. Holman, A. Descoeudres, S. D. Wolf, C. Ballif, IEEE J. Photovolt. 2013, 3, 1243.
- [19] L. Senaud, G. Chrismann, A. Descoeudres, J. Geissbühler, L. Barraud, N. Badel, C. Allebe, S. Nicolay, M. Despeisse, B. P. Salomon, C. Ballif, IEEE J. Photovolt. 2019, 9, 1217.

- [20] Z. C. Holman, S. D. Wolf, C. Ballif, Light: Sci. Appl. 2013, 2, e106.
- [21] F.J. Huang, T. Soderstrom, O. Cubero, V. Terrazzoni-Daudrix, C. Ballif, J. Appl. Phys. 2008, 104, 064509.
- [22] L. Zeng, Y. Yi, C. Hong, J. Liu, N. Feng, X. Duan, L. C. Kimerling, B. A. Alamariu, Appl. Phys. Lett. 2006, 11, 1111111.
- [23] M. Peters, M. Rüdiger, H. Hauser, M. Hermle, B. Bläsi, Prog. Photovolt. Res. Appl. 2012, 20, 862.
- [24] A. Melor, H. Hauser, C. Wellens, J. Benick, J. Eisenlohr, M. Peters, A. Guttowski, I. Tobias, A. Marti, A. Luque, B. Bläsi, Opt. Express 2013, 21, A295.
- [25] S. E. Han, G. Chen, Nano Lett. 2010, 10, 4962.
- [26] A. Ingenito, S. Luxembourg, P. Spinelli, A. Weeber, O. Isabella, M. Zeman, presented at *Proc.42nd IEEE PVSC*, New Orleans, LA, June 2015.
- [27] M. Tucci, L. Serenelli, E. Salza, L. Pirozzi, G. D. Cesare, D. Caputo, M. Ceccarelli, Mat. Sci. Eng. B 2009, 159–160, 48.
- [28] J. Krc, M. Zeman, S. L. Luxembourg, M. Topic, Appl. Phys. Lett. 2009, 94, 153501.
- [29] Z. C. Holman, A. Descoeudres, L. Barraud, F. Z. Fernandez, J. P. Seif, S. D. Wolf, C. Ballif, IEEE J. Photovolt. 2012, 2, 7.
- [30] T. Söderström, Y. Yao, R. Grischke, M. Gragert, B. Demaurex, B. Strahm, P. Papet, H. Mehlich, M. Koenig, A. Waltinger, J. Zhao, J. Krause, presented at *Proc.42nd IEEE PVSC*, New Orleans, LA, June 2015.
- [31] A. Faes, in Cell Processing, Methallization and Internaconnection, 2018, p. 65.